






## Skilful predictions of the Summer North Atlantic Oscillation

Nick Dunstone <sup>1</sup>✉, Doug M. Smith <sup>1</sup>, Steven C. Hardiman<sup>1</sup>, Leon Hermanson <sup>1</sup>, Sarah Ineson<sup>1</sup>, Gillian Kay<sup>1</sup>, Chaofan Li<sup>2</sup>, Julia F. Lockwood<sup>1</sup>, Adam A. Scaife <sup>1,3</sup>, Hazel Thornton<sup>1</sup>, Mingfang Ting <sup>4</sup> & Lei Wang<sup>5</sup>

The Summer North Atlantic Oscillation is the primary mode of atmospheric variability in the North Atlantic region and has a significant influence on regional European, North American and Asian summer climate. However, current dynamical seasonal prediction systems show no significant Summer North Atlantic Oscillation prediction skill, leaving society ill-prepared for extreme summers. Here we show an unexpected role for the stratosphere in driving the Summer North Atlantic Oscillation in both observations and climate prediction systems. The anomalous strength of the lower stratosphere polar vortex in late spring is found to propagate downwards and influence the Summer North Atlantic Oscillation. Windows of opportunity are identified for useful levels of Summer North Atlantic Oscillation prediction skill, both in the 50% of years when the late spring polar vortex is anomalously strong/weak and possibly earlier if a sudden stratospheric warming event occurs in late winter. However, we show that model dynamical signals are spuriously weak, requiring large ensembles to obtain robust signals and we identify a summer ‘signal-to-noise paradox’ as found in winter atmospheric circulation. Our results open possibilities for a range of new summer climate services, including for agriculture, water management and health sectors.

<sup>1</sup>Met Office Hadley Centre, Exeter, UK. <sup>2</sup>Center for Monsoon System Research, Institute of Atmospheric Physics, Chinese Academy of Sciences, Beijing 100029, China. <sup>3</sup>Department of Mathematics and Statistics, University of Exeter, Exeter, UK. <sup>4</sup>Lamont-Doherty Earth Observatory, Columbia University, Palisades, NY, USA. <sup>5</sup>Department of Atmospheric and Oceanic Sciences & Institute of Atmospheric Sciences, Fudan University, Shanghai, China.  
✉email: [nick.dunstone@metoffice.gov.uk](mailto:nick.dunstone@metoffice.gov.uk)

Skilful predictions of seasonal climate variability that can be used by government and industry planners are important for a resilient society. In our rapidly changing climate this need is increasingly important as interannual variability can either mask or exacerbate the climate impacts due to global warming. The summer season is of particular concern given the increasing frequency and severity of heatwaves<sup>1</sup> and drought conditions that can negatively impact agriculture, human health and water resources. In the North Atlantic sector, European and North American summer climate variability are partly driven by large-scale modes of atmospheric circulation. Whilst less studied than in winter, some progress has been made in understanding/predicting the second most dominant mode of variability, the Summer East Atlantic (SEA) pattern. Studies have linked the SEA pattern to both heating anomalies in the sub-tropical Pacific/Caribbean regions<sup>2,3</sup> and to precursor sea surface temperature (SST) anomalies in the North Atlantic<sup>4</sup>. North Atlantic sector summer climate variability has also been linked to decadal variability in North Atlantic SSTs<sup>5,6</sup>. However, the drivers and seasonal predictability of the dominant mode of North Atlantic circulation variability, the Summer North Atlantic Oscillation (SNAO<sup>7</sup>), are still largely unknown.

The summer (June–August, JJA) observed SNAO pattern is shown in Fig. 1a (see Methods), and accounts for 37% of the regional variance in mean sea level pressure over the 1979–2022 period. We note that this is significantly more than the 22% reported previously<sup>8</sup> over an earlier period (1899–2001) and is explained by increased SNAO variance from 2007. The SNAO pattern is shifted poleward and tilted with respect to the winter NAO, with centres of action over Greenland and north-west Europe. As in winter, the SNAO is intimately linked with the position and strength of the North Atlantic jet streams and storm tracks<sup>9</sup>. A positive (negative) phase of the SNAO represents a northward (southward) shift of the tropospheric jets (Fig. 1b) which show coherence not just across the North Atlantic sector but also across the Eurasian continent to East Asia (Fig. 1b, c). The SNAO has profound surface climate impacts over north-west Europe (Fig. 1d, e), for example the UK is strongly impacted by the SNAO due to its location at the southern SNAO node (correlation  $r = -0.77$  with UK observed rainfall and  $r = 0.53$  with detrended temperature over 1979–2022<sup>10</sup>). Significant SNAO correlations are also found with surface climate over south-eastern Europe<sup>11</sup>, North America<sup>12</sup> and central China<sup>13</sup>.

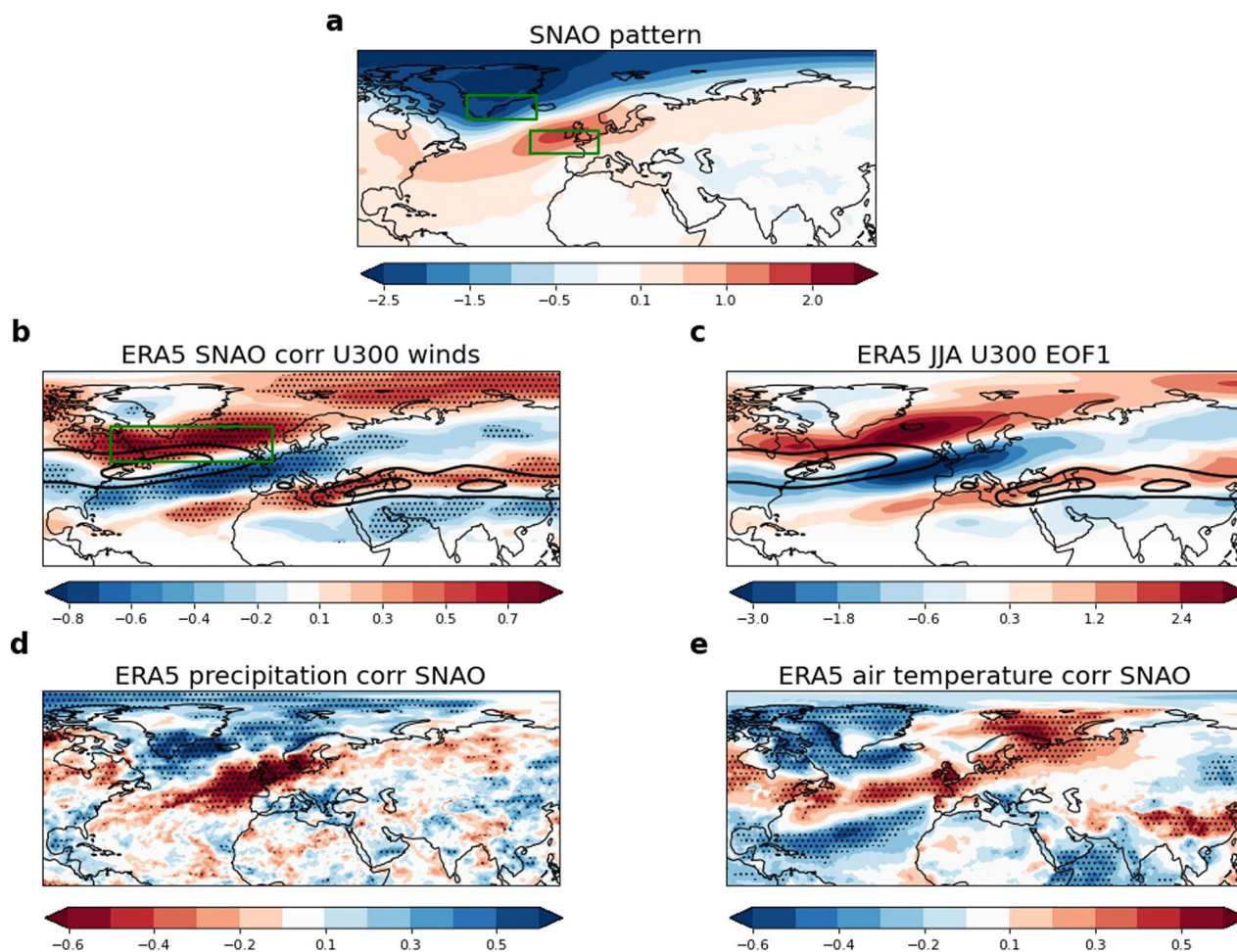


**Fig. 1** Characterising the observed SNAO, its relationship to jet variability and surface summer climate impacts. **a** MSLP regressed on to the 1st principal component associated with the 1st EOF of summer ERA5 MSLP calculated over the North Atlantic domain [90E–40W, 20–70 N] and accounting for 37% of the variance. Green boxes show regions used to calculate SNAO index<sup>25</sup>. **b** the SNAO index correlated with the field of ERA5 upper level 300 hPa winds. Green box shows region used to calculate North Atlantic sector winds for cross-section plots in Figs. 3a, b and 5a. **c** the 1st EOF of upper level 300 hPa winds calculated over the extended domain shown and accounting for 20% of the variance. Contours in (**b**, **c**) are climatological 300 hPa zonal wind to highlight the position of the jets (contours plotted at 15 and 20 m/s). The SNAO index correlated with the ERA5 fields of summer precipitation (**d**) and linearly detrended 2 m air temperature (**e**). Stippling shows correlations significantly different from zero at the 90% confidence level according to a 2-sided Student's *t* test.

Key advances have been made in the last decade in predicting the winter North Atlantic Oscillation on seasonal<sup>14–16</sup>, interannual<sup>17</sup> and decadal<sup>18</sup> timescales using dynamical initialised near-term climate prediction systems. In contrast, however, these systems do not show significant skill for the SNAO<sup>19</sup>. For example, the eight seasonal prediction systems in the C3S archive assessed over 1993–2016 (see Methods) have SNAO prediction skill ranging from  $r = -0.32$  to  $r = 0.04$  and even the multi-model mean (202 members) shows negative skill ( $r = -0.19$ )<sup>19</sup>. There are good physical reasons why we may expect extratropical boreal summer circulation to be less predictable than winter<sup>20,21</sup>. Boreal summer coincides with reduced amplitude tropical Pacific El Niño Southern Oscillation (ENSO) variability. During winter ENSO drives extratropical climate predictability via the poleward propagation of planetary waves<sup>22</sup>, however these are partly inhibited in summer by the development of climatological easterly winds in the sub-tropics. Finally, whilst stratosphere-troposphere coupling plays a key role in winter circulation predictability<sup>23,24</sup> it was not previously thought to influence the SNAO given the stratospheric polar vortex collapse prior to summer<sup>21</sup>. However, this view was recently challenged when a significant empirical correlation was noted between the observed late spring stratosphere and the SNAO<sup>25</sup>. Here we use large ensembles of near-term climate predictions, and perturbation experiments, to identify that a robust and causal influence of the stratosphere on the SNAO exists, to understand the mechanism and assess windows of opportunity for skilful real-time SNAO prediction.

## Results

**Stratospheric precursor to SNAO in observations and climate model simulations.** We search for possible circulation precursors to the SNAO by correlating the zonal mean zonal wind in May with the SNAO index. We examine both ERA5 reanalysis<sup>26</sup> and the retrospective predictions (hindcasts) of the Met Office DePreSys3<sup>17</sup> (hereafter the ‘model’, see Methods) near-term climate prediction system starting every 1st May over the 44 year period 1979–2022 (Fig. 2a, b). We find significant correlations in the May polar stratosphere (>60 N) in both ERA5 and the model ensemble mean, whereas in contrast only weaker correlations are found in the troposphere. This suggests that an anomalously strong stratospheric polar vortex in May could drive a positive SNAO, corresponding to a stronger and poleward shifted summer North Atlantic jet. This is consistent with our understanding of stratosphere-troposphere coupling in winter months<sup>27,28</sup> whereby an anomalous strengthening (weakening) of the polar vortex exerts a lagged downward influence promoting westerly (easterly) tropospheric wind anomalies in mid-latitudes. To further quantify this unexpected stratospheric influence, we create a May polar vortex index (MPVI) in the lower stratosphere (50 hPa, see Fig. 2a, b and Methods) and find significant correlations to the SNAO in observations  $r = 0.38$  ( $p = 0.01$ ) and the model ensemble mean  $r = 0.43$  ( $p < 0.01$ ). However, a direct model-observation comparison would use individual model ensemble members, and so we produce a distribution (Fig. 2c) showing the range of possible MPVI-SNAO correlations in single member realisations (see Methods). On average, we find only a weak MPVI-SNAO correlation in the ensemble members ( $r = 0.1$ ,  $p = 0.5$ ) and the observed correlation is outside the model 5–95% range, suggesting a spuriously weak model teleconnection. As a result, large ensemble sizes needed to be averaged to extract the predictable signal and hence reveal a robust relationship (Fig. 2d). We also assess this MPVI-SNAO relationship in the NCAR SMYLE<sup>29</sup> near-term prediction system (which also has 1st May hindcasts over 1979–2019, see Methods). We again find a robust

relationship ( $r = 0.32$ ,  $p = 0.04$ —green star in Fig. 2d) which is close to that from DePreSys3 when allowing for the reduced ensemble size.

This robust connection between the late spring stratosphere and the SNAO in observations and two climate prediction systems is unexpected due to the breakdown of the polar vortex in boreal spring<sup>21</sup> after which winds become easterly, prohibiting subsequent vertical propagation of Rossby waves<sup>30</sup> and further stratosphere-troposphere coupling. This ‘final warming’ is driven by a combination of the seasonal increase in radiative heating of the polar region and variability in the dynamical upward planetary wave activity. At the 10 hPa level, commonly used to measure polar vortex strength and monitor sudden stratospheric warming (SSW) events, the mean final warming date is at the end of April<sup>31</sup> so a downward influence on the SNAO might seem unlikely given its characteristic 2–4 week propagation timescale. However, because the seasonal increase in radiative heating first happens in the upper stratosphere, the vortex essentially collapses from the top-down. The vortex can therefore persist<sup>32</sup> in the lower stratosphere (50 hPa) where the mean final warming date is almost a month later in late May<sup>31</sup> and can be as late as mid-June. Indeed, we find a robust correlation ( $r = 0.60$ ,  $p < 0.001$ ) between the MPVI and the final warming date at 50 hPa, indicating that an anomalously strong MPVI corresponds to a late breakdown of the stratospheric polar vortex and vice-versa.

## Downward propagation and the early summer North Atlantic jet.

The mechanisms whereby information descends from the stratosphere to impact the surface have been studied for several decades. An anomalously strong/weak vortex provides a positive/negative potential vorticity (PV) anomaly that needs to be eroded before an SSW, or final stratospheric warming, can take place. This means that, for a given source of polewards PV flux from Rossby wave breaking, the timing of the resulting SSW (or final warming) will be modulated accordingly. It is now understood that whilst the direct tropospheric impact of a stratospheric signal would be small<sup>33,34</sup>, eddy feedback within the troposphere acts to generate the magnitude and spatial nature of the observed tropospheric response<sup>28,35–37</sup>. In particular, the shift in latitude of the tropospheric jet in response to perturbations to the stratospheric polar vortex strength requires dynamical feedback<sup>38</sup>. These mechanisms apply to stratospheric final warmings just as they do to SSWs. Indeed, the different surface impacts of early and late (or dynamical and radiative) final warmings on the surface have been previously noted<sup>31,39,40</sup>.

We assess the downward influence by correlating the MPVI with the summer North Atlantic sector monthly mean zonal winds (green box in Fig. 1b). Both the observed and model ensemble mean again show significant correlations in the May stratosphere only and then a downward propagation of the signal into the troposphere in June (Fig. 3a, b). This is particularly clear in the model ensemble mean and significant correlations persist into July but weaken by August. To examine the spatial structure of the downwards signal we plot correlation maps of MPVI with summer upper troposphere zonal winds (U300, Fig. 3c, d). In both the observations and model we find that positive MPVI drives a northward shift of the jet, as expected for a positive phase of the SNAO (c.f. Fig. 1b), and similarly coherent circulation anomalies stretching across the Eurasian continent.

To further probe the causality of the MPVI-SNAO connection, we perform a simple perturbation experiment to isolate this atmospheric mechanism from that driven by predictable changes in the ocean. We select a year with near neutral MPVI and SNAO and replace only the atmosphere initial conditions on 1st May with those from the three strongest and weakest MPVI years (see



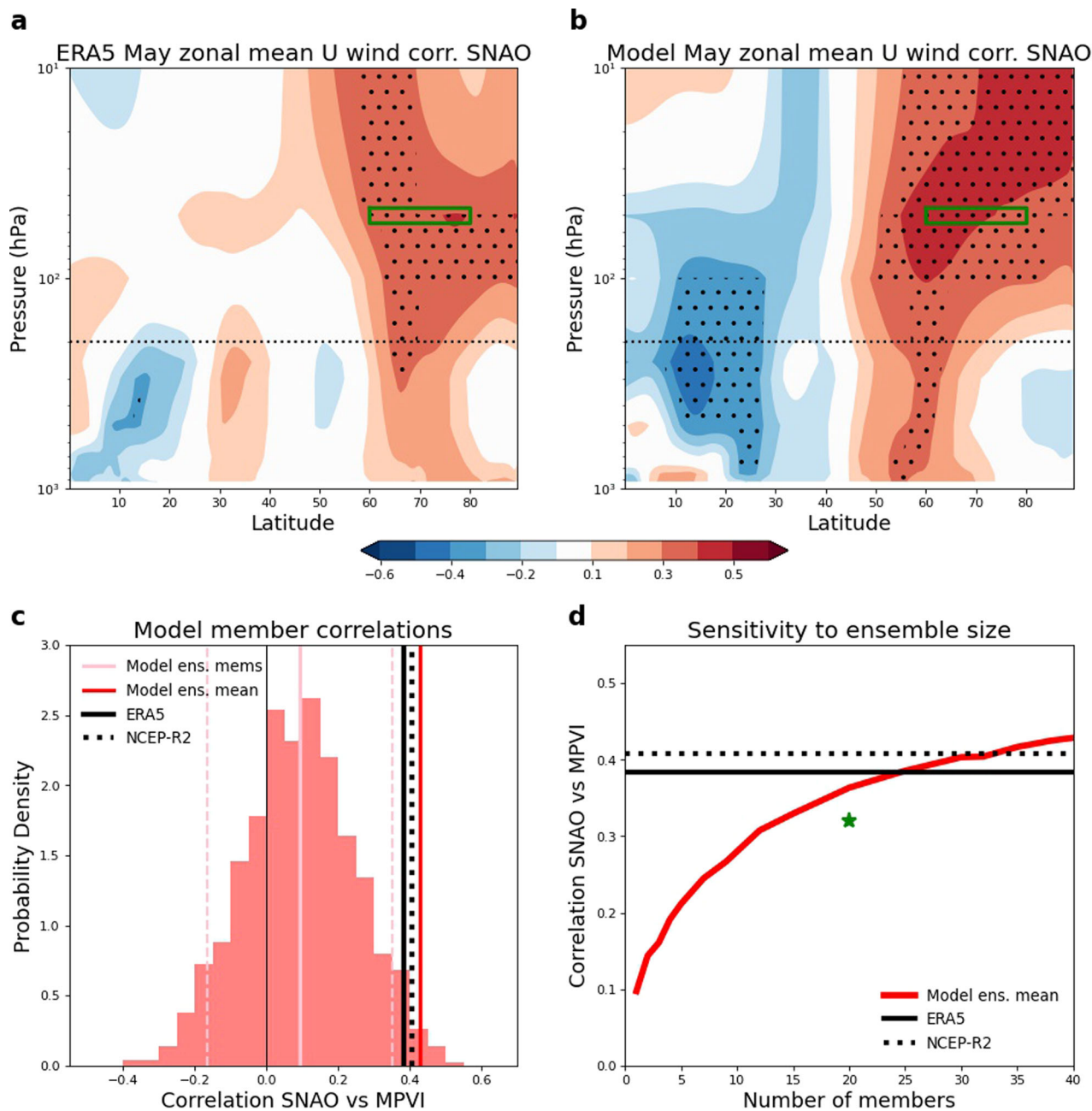


**Fig. 2 Precursor SNAO signals in the late spring stratosphere.** SNAO index correlated with the preceding May zonal mean zonal winds plotted as a latitude-height cross-section in ERA5 (**a**) and the model ensemble mean (**b**). Dashed horizontal line shows the approximate location of the tropopause, green boxes show the location of the box used to define the MPVI and stippling shows correlations significantly different from zero at the 95% confidence level according to a two-sided Student's *t* test. **c** Histogram showing the distribution of model member correlations between the MPVI and SNAO. Pink solid and dashed vertical lines show the mean of the model member correlations and the 5-95% interval respectively, red vertical line shows the ensemble mean MPVI vs SNAO correlation and the black vertical lines shows the equivalent observed estimates from ERA5 and NCEP-R2 reanalyses<sup>62</sup>. **d** The strength of the SNAO vs MPVI correlation (red curve) as a function of ensemble size, with the black horizontal line showing the equivalent observed ERA5 and NCEP-R2 values. The green star shows the strength of SNAO vs MPVI correlation using the NCAR-SMYLE<sup>29</sup> prediction system for comparison (see Methods).

Methods). The results of the experiment do indeed support a causal link, showing a significant circulation response (Fig. 3e) with a northward shift of the North Atlantic jet (i.e. a positive SNAO) being driven by positive MPVI anomalies.

#### Real-time SNAO prediction and windows of opportunity.

Despite identifying a robust causal mechanism, we note that the observed MPVI would be unknown until after the start of June

and so could not be used for real-time SNAO predictions ahead of summer. However, due to high stratospheric monthly predictability, MPVI is very well predicted by the model ensemble mean ( $r = 0.91$ ) and hence MPVI predictions available in early May can be used as a real-time predictor of observed SNAO (Fig. 4a,  $r = 0.40$ ,  $p = 0.01$ ). Whilst statistically significant, this is a modest level of skill and hence of limited value to users. However, significant MPVI anomalies do not occur every year and so we re-evaluate skill for the almost half of years (21 of 44)

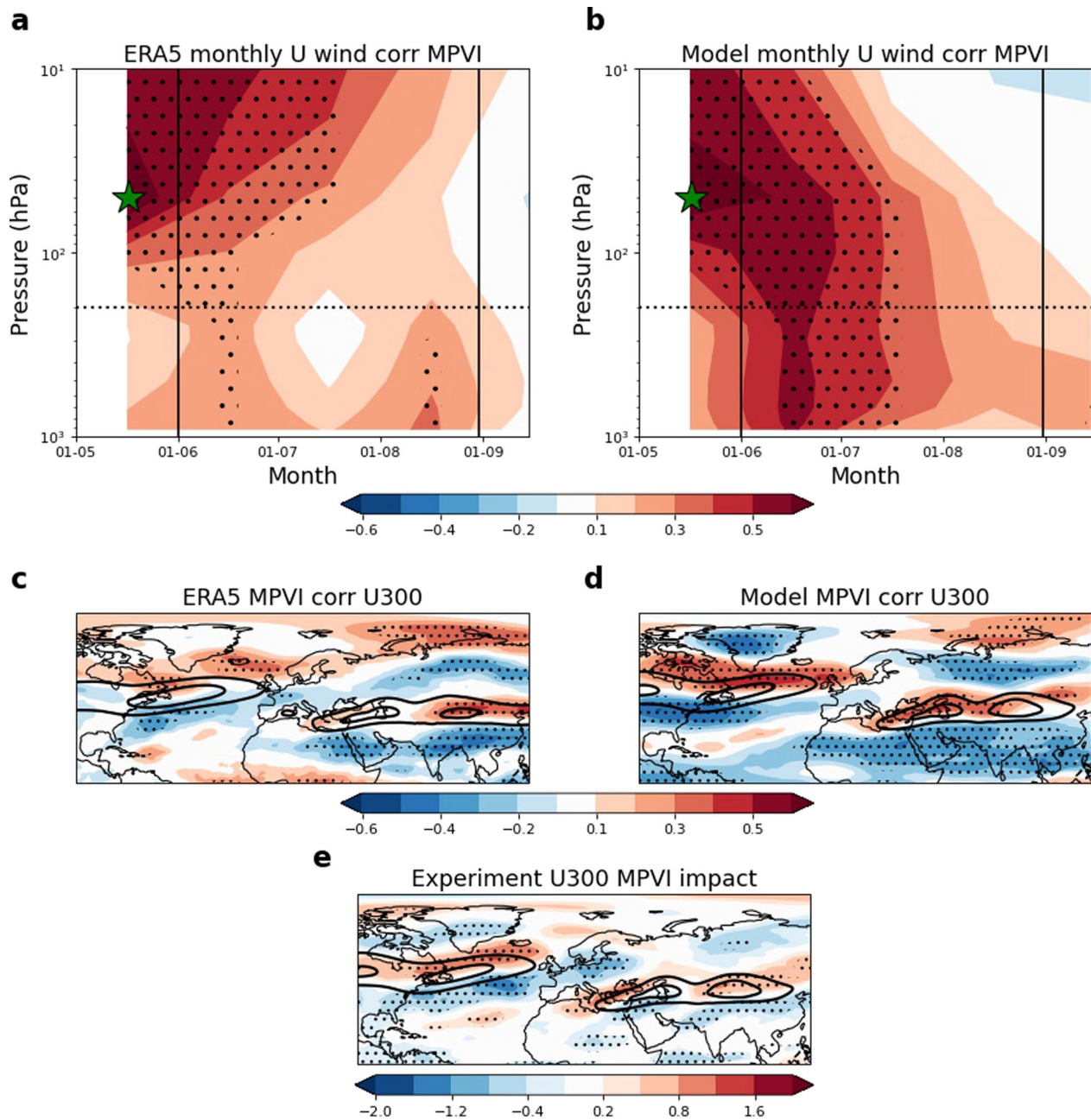


**Fig. 3 Downward propagation of late spring stratospheric anomalies.** MPVI correlated with the monthly zonal mean winds over the North Atlantic sector (50–65 N, green box in Fig. 1b) plotted as a latitude-height cross-section in ERA5 (a) and the model ensemble mean (b). Solid vertical lines indicate the start and end of boreal summer, dashed horizontal line shows the approximate location of the tropopause, green stars indicate the location of the MPVI. MPVI correlated with subsequent summer upper level 300 hPa zonal winds in ERA (c) and model ensemble mean (d), contours are climatological 300 hPa zonal wind to highlight the position of the jets (contours plotted at 15 and 20 m/s). Stippling in (a–d) shows correlations significantly different from zero at the 90% confidence level according to a two-sided Student’s *t* test. e Impact of the MPVI on summer upper level 300 hPa zonal winds as diagnosed by perturbation experiments that switch atmospheric initial states to separate atmosphere and ocean drivers (Methods). Differences (m/s) are plotted between the average of the three positive and three negative MPVI states and stippling shows locations where these are significant at the 95% confidence level.

when the MPVI is forecast to be ‘active’ (>1 m/s anomaly). We then obtain a higher level of skill ( $r = 0.55$ , Fig. 4a) with the hit rate also increasing from 61% to 71% for predicting the SNAO sign. Hence approximately every other year, we can expect a window of opportunity to make a potentially useful SNAO prediction.

Earlier, we highlighted that eight operational seasonal prediction systems have no significant skill for dynamical SNAO predictions (over 1993–2016) and we find the same here over the

longer 1979–2022 period, as shown in Fig. 4b ( $r = 0.22$ ,  $p = 0.15$ ). However, we use our new understanding of the role of the late spring stratosphere to re-evaluate dynamical SNAO skill using only the 21 years with a forecast active MPVI and find improved and significant skill  $r = 0.42$  ( $p = 0.05$ , Fig. 4b). Whilst this is still lower than the  $r = 0.55$  obtained from using the predicted MPVI as a predictor for the observed SNAO, it is a marked improvement. Differences primarily arise from a small number of years, e.g. 2006 where the model SNAO did not follow the

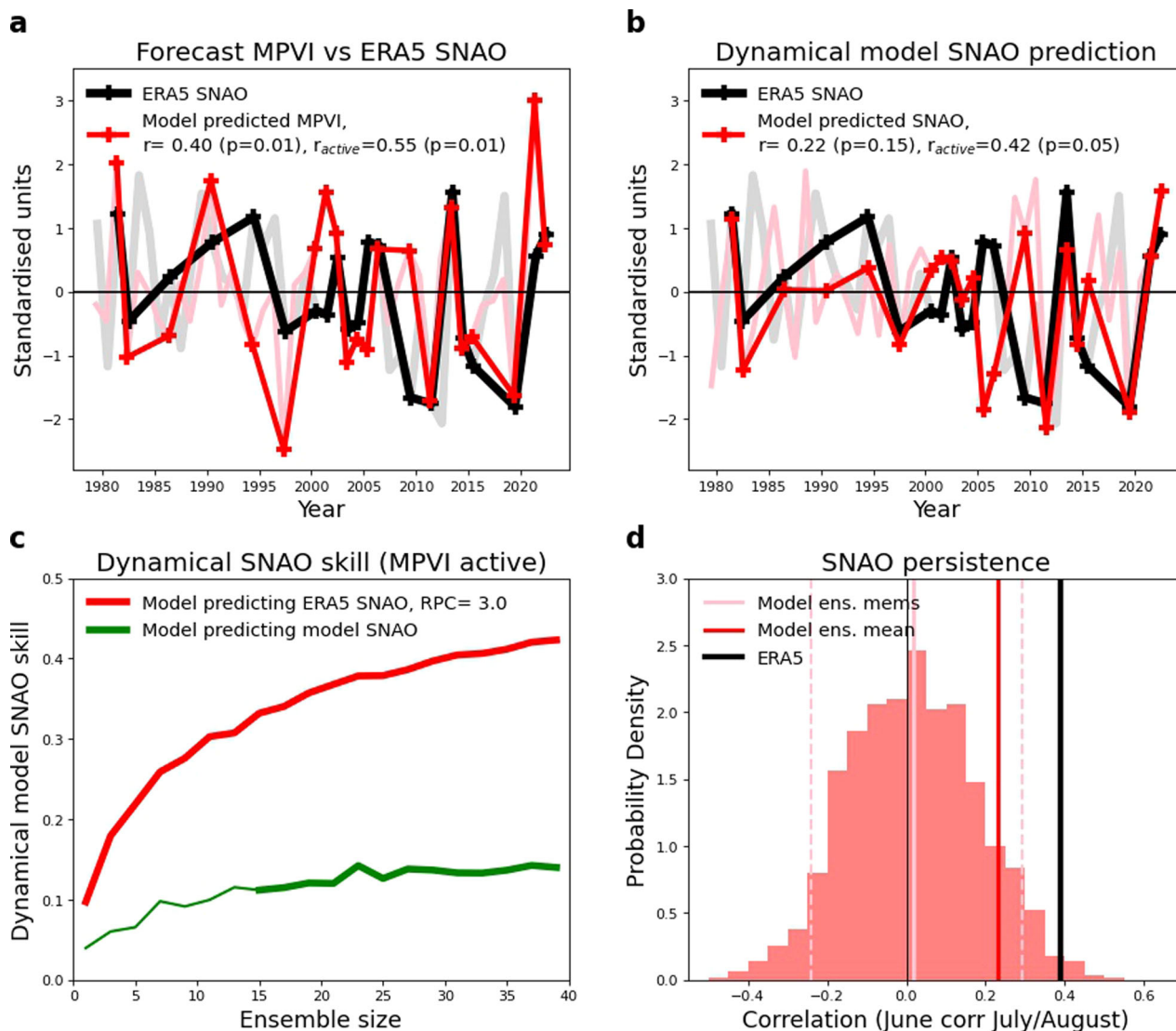


**Fig. 4** Windows of opportunity for skilful SNAO prediction and spuriously weak model signals. Standardised timeseries of ERA5 SNAO and the model predicted MPVI (a) and the model predicted SNAO (b). In both panels, all years are shown in the background, whilst the 21 years where the model predicted MPVI is ‘active’ ( $> \pm 1$  m/s) are plotted in the foreground. c model SNAO skill in predicting ERA5 SNAO (red) and itself (i.e. perfect predictability, green) as a function of ensemble size during active MPVI years. The switch to a thicker green line indicates the ensemble size where the model skill in predicting the observed SNAO is significantly higher than the skill of the model predicting itself. d histogram showing the distribution of the strength of SNAO persistence through the summer measured by SNAO in June correlated with SNAO in July/August. Solid and dashed vertical lines show the model member mean average and 5–95% intervals, respectively, the solid red vertical line shows the ensemble mean persistence and the vertical black line shows the ERA5 SNAO persistence.

predicted MPVI index, and further investigation may be fruitful to understand this.

Given significant dynamical SNAO skill during active MPVI years, we can now assess whether spuriously weak summer predictable signals are present as found for winter North Atlantic circulation<sup>14–17,41,42</sup>. We find that the skill of the model SNAO in predicting the real-world SNAO rises slowly as a function of ensemble size (Fig. 4c) and is still increasing at 40 members. However, the average skill of the model ensemble in predicting itself (a single randomly chosen member) is significantly lower (Fig. 4c, green line) with correlation of only  $r = 0.14$ . This is very similar to that found for seasonal predictions of the winter NAO<sup>16,17,42</sup> with the model having higher skill in predicting the real-world than itself. This ‘signal-to-noise paradox’ implies spuriously weak predictable forced model signals relative to the internal noise and can be quantified by calculating the ratio of

predictable components (RPC, see Methods) with an  $RPC > 1$  indicating weak model forced signals. We find  $RPC = 3.0$  for dynamical SNAO predictions during active MPVI years, similar to seasonal winter NAO predictions ( $RPC = 2.3$ )<sup>17</sup>.

Understanding the source of the winter signal-to-noise paradox has been an active research endeavour for almost a decade now. One of the currently favoured explanations is that weak model atmospheric eddy feedback<sup>43,44</sup> may give spuriously weak predictable signals. This could also explain the weak SNAO signals found here but other hypotheses include weak model ocean-atmosphere coupling<sup>4</sup>. One conceptual picture of the signal-to-noise paradox, consistent with either weak model eddy feedback or ocean-atmosphere coupling, is that the model has a reduced persistence of atmospheric circulation ‘regimes’<sup>45</sup>. We assess the persistence of the SNAO through the summer months by correlating the SNAO calculated in June with that in



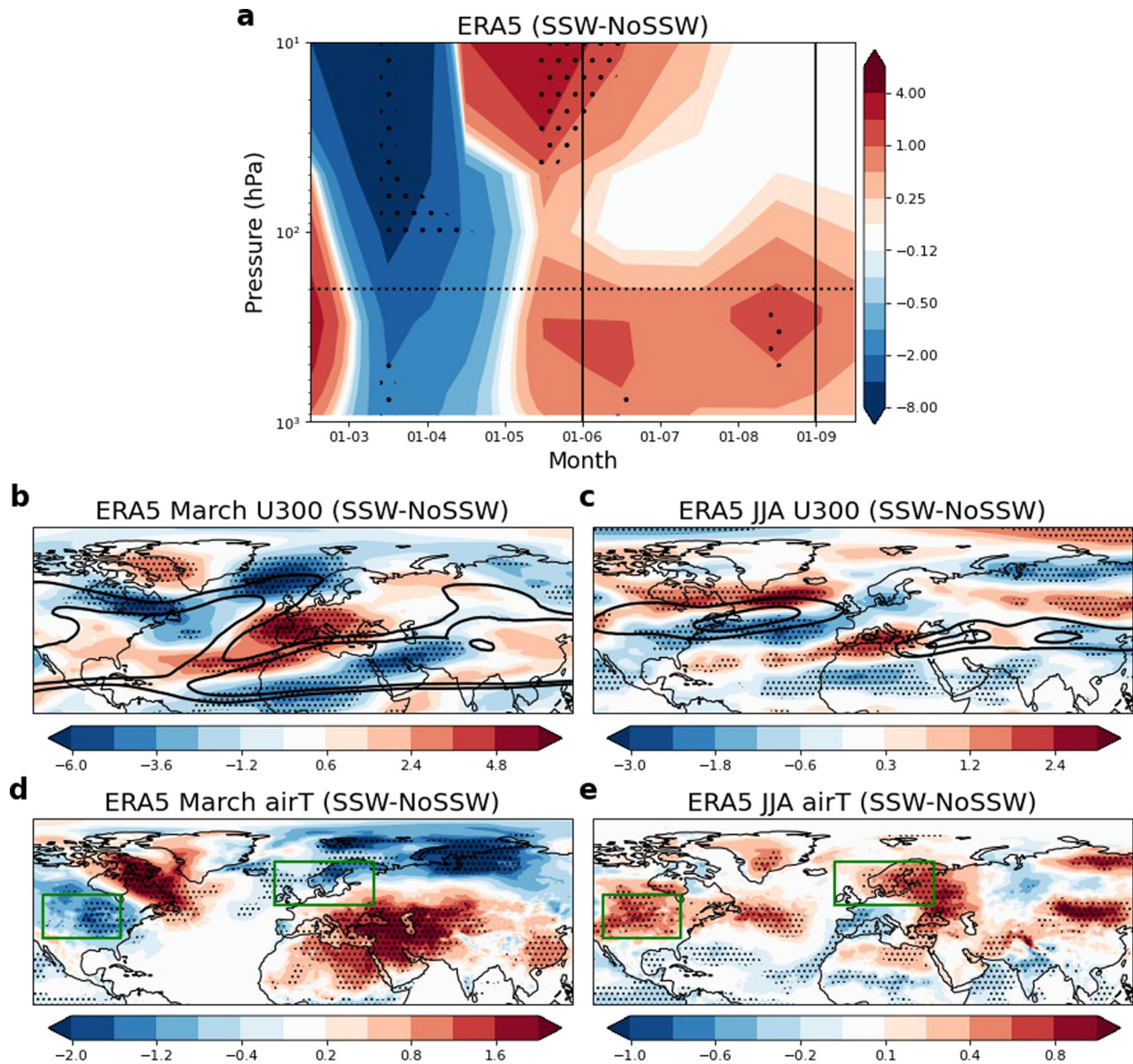


**Fig. 5 Long-lasting influence of a late winter SSW.** All panels are composite differences of observed ERA5 data for the 12 years in which an SSW occurred between 1st February and 15th March against the remaining 32 years (see Methods). **a** the composite difference for monthly zonal mean winds (m/s) over the North Atlantic sector (50–65N, green box in Fig. 1b) plotted as a latitude-height cross-section in ERA5 from February through to September. Composite differences for ERA5 upper troposphere 300 hPa zonal winds (m/s) in March (**b**) and summer (**c**), contours are climatological 300 hPa zonal wind to highlight the position of the jets (contours plotted at 15 and 20 m/s). Composite differences for ERA5 detrended 2 m air temperature (K) in March (**d**) and summer (**e**), green boxes highlight North America and Northern Europe which both transition from significant cold anomalies in March to warm ones in summer. Stippling on all panels shows significant differences at the 90% confidence level as assessed using a one-sided Student's *t* test.

July–August using all 44 years. Across individual model members we find very weak persistence of SNAO from June to July–August (Fig. 4d,  $r = 0.02$  with a 5–95% range of  $r = -0.23$  to  $r = 0.29$ ), whereas the observed persistence is much stronger ( $r = 0.39$ ), as is the model ensemble mean ( $r = 0.23$ ). Hence model members appear to have spuriously weak SNAO persistence, which should be explored further to understand the source of the SNAO signal-to-noise paradox.

**Connection to late winter SSWs.** Whilst much of the MPVI may be driven by internal variability, it is interesting to consider possible pre-cursor behaviour. Here we explore whether a late winter SSW event, the most extreme example of stratosphere polar vortex variability, may drive subsequent MPVI variability

using observed reanalysis data. We identify 12 observed SSW events that occur in late winter between 1st February and the 15th March that are distinct from the ‘final warming’<sup>46,47</sup> (see Methods). We calculate the composite difference between the evolution of these years and the other 32 years for North Atlantic circulation (Fig. 5). As expected, easterly stratospheric wind anomalies associated with the SSW are seen in February/March and these propagate down with the typical 2–4 week timescale to drive easterly tropospheric wind anomalies in March/April (Fig. 5a, b), consistent with a negative winter NAO. These easterly wind anomalies act to reduce the upward wave flux, which reduces the dynamical heating in the stratosphere. Hence, as the upper stratosphere cools radiatively after the SSW, it overshoots the climatological temperature<sup>48</sup>, resulting in an anomalously strong polar vortex seen at 10 hPa in April. This signal descends to the

lower stratosphere in May giving a positive MPVI. Then, consistent with the evolution described in this paper, there is a downward propagation of this westerly signal into early summer giving a poleward shifted North Atlantic summer jet (Fig. 5a, c) consistent with a positive SNAO, which persists throughout the summer.

An SSW occurring sometime in late winter can therefore have a significant and long-lasting impact via two-way stratosphere-troposphere coupling that can potentially connect surface climate anomalies in late winter/early spring to those throughout the summer. Hence late winter SSWs are windows of opportunity for extended range seasonal prediction and in some regions can increase the probability for a particular sequence of climate anomalies. For example, in Fig. 5d, e, we show the air temperature composite differences and highlight the North American and Northern Europe regions. In March, we find temperature anomalies matching the well-known ‘quadrupole pattern’ produced by the NAO, albeit shifted slightly poleward due to the climatological position of the March extratropical jet. The negative NAO induced by the SSW drives anomalously cold conditions in both North America and Northern Europe. However, a few months later during summer, both regions experience anomalously warm conditions due to the northward shift of the jet associated with a positive SNAO. This increased risk of a cold early spring to warm summer transition during years with late SSWs could be useful for many users, such as the agriculture sector to adjust time of planting/harvesting or to choose the most suitable crop varieties. Summer 2018 is the last example of such a year where a late winter SSW occurred<sup>49</sup>, driving a very cold March over Northern Europe, followed by a very warm summer associated with a positive SNAO<sup>50</sup>.

## Discussion

We have shown that skilful predictions of the SNAO are possible one month ahead of summer. This is a significant advance in our ability to make useful seasonal predictions of summer climate variability over parts of Northern Europe, North America and East Asia. Whilst a role for the stratosphere in driving summer circulation was somewhat unexpected a priori, we now have robust evidence from observations<sup>25</sup> and climate model simulations/experiments that significant polar vortex anomalies in the May lower stratosphere can exert a significant downward influence on the SNAO. By analogy with the popular ‘dripping paint’ description of winter stratosphere-troposphere coupling<sup>27</sup>, here we are seeing the ‘final drip’ from the paint pot. We have shown that this downward propagation, as in winter, drives tropospheric North Atlantic jet anomalies in early summer which can then persist. In fact, the subsequent complete breakdown of the stratospheric polar vortex may indeed increase the long-term persistence of that final stratosphere forcing by inhibiting further stratospheric influence.

The high skill for month ahead stratospheric variability means we can use the predicted MPVI to make real-time SNAO predictions. The ~50% of years that exhibit large MPVI anomalies represent windows of opportunity to make SNAO predictions with sufficient skill for some user applications. Furthermore, analysis of observed reanalysis suggests that a late winter SSW may provide a rarer but valuable window of opportunity to link late winter and early spring surface regional climate anomalies with those up to the end of the summer. As a near-term prediction community, we need to be monitoring for, and taking advantage of, such windows of opportunity to issue more confident forecasts and warnings of impending climate extremes when possible<sup>51</sup>. Having the physical understanding of the driving mechanism, e.g. as shown here for the stratosphere-SNAO

influence, is key to building our forecast confidence, especially where insufficient hindcasts exist to fully assess flow/state dependent skill. We need to develop new tools and methods to take full advantage of these windows of opportunity<sup>52</sup>.

Whilst we find dynamical model SNAO predictions are skilful during the half of years with significant MPVI anomalies exist, we note that the lack of skill across all years suggests some other drivers of summer circulation may not be well captured and requires further investigation<sup>19,53</sup>. However, during forecast active MPVI years we have shown the first clear evidence for a signal-to-noise paradox in summer circulation, mirroring that found in wintertime. Understanding the origin of weak model extratropical circulation signals is a key research priority given that it may have implications not only for near-term climate predictions but also for longer timescale climate projections<sup>42</sup>. At present though, the key to skilful seasonal SNAO predictions is using systems with well resolved/initialised stratosphere components and large ensemble sizes to robustly extract the weak model predictable signals. We can, therefore, exploit windows of opportunity for skilful SNAO predictions and hence develop regional summer climate services for users.

## Methods

**Observed data and indices.** We use the ERA5 reanalysis<sup>26</sup> from 1979 to 2022 for all observation based data, except for when comparing the UK mean rainfall and detrended temperature relationship with the observed SNAO where we use the Met Office HadUK-Grid dataset<sup>10</sup>.

The SNAO index is that used previously<sup>25</sup> calculated using the difference between two boxes (25°W–5°E, 45–55°N) and (52–22°W, 60–70°N) as shown in Fig. 1a. We define a May Polar Vortex Index (MPVI) to represent the strength of the May monthly mean polar vortex in the lower stratosphere by calculating a zonal mean zonal wind at 50 hPa over the latitudes 60–80°N as shown in Fig. 2a, b.

**Sampling model members and signal-to-noise.** The distribution of possible MPVI-SNAO correlation strengths in model members (Fig. 2c), and the strength of SNAO persistence (June SNAO correlated with July–August SNAO), are both assessed by randomly sampling ensemble members for each hindcast year independently without replacement. We note that members from one hindcast year have no physical relationship with the same member in a different hindcast year, which means that a very large number of permutations are possible and we perform 1000 trials. We perform a similar sampling procedure to assess the sensitivity to ensemble size of both the MPVI-SNAO relationship (Fig. 3d) and the SNAO skill during forecast active MPVI years (Fig. 4c).

The SNAO signal-to-noise paradox is characterised by the ratio of predictable components (RPC) for dynamical model SNAO predictions during forecast active MPVI years and is calculated as follows<sup>41</sup>:

$$RPC = \frac{PC_{obs}}{PC_{mod}} \geq \frac{r_{mo}}{\sqrt{\sigma_{sig}^2 / \sigma_{tot}^2}}$$

where the predictable component (PC) of the real world ( $PC_{obs}$ ) can be conservatively estimated by the hindcast variance explained ( $r_{mo}^2$ ) and the predictable component of the model may be estimated by the variance of the ensemble mean ( $\sigma_{sig}^2$ ) divided by the variance of single ensemble members ( $\sigma_{tot}^2$ ). The square root is taken for convenience. We note that the RPC can also be calculated as the ratio<sup>42</sup> of the skill in the model predicting the real-world SNAO (0.42) to that of the model predicting its own SNAO (0.14), as shown in Fig. 4c, which also gives



RPC = 3.0. These two formulations for calculating RPC converge to the same result given sufficiently large ensemble sizes, as found here.

**Climate prediction systems.** The main climate prediction system used in this study is the Met Office DePreSys3 system as it has a long hindcast period (1979–2022) for 1st May start dates, a large 40 member ensemble size and is available to the authors to run perturbation experiments with (see below). DePreSys3 has also been shown to have good skill in predicting the winter NAO<sup>17</sup>. DePreSys3 uses the Hadley Centre Global Environmental Model version 3 at the Global Coupled model 2.0 (HadGEM3-GC2)<sup>54</sup> configuration which is the same model (and resolution) as used in the Met Office GloSea5 operational seasonal prediction system<sup>55</sup>. It has atmospheric resolution of 0.83° longitude by 0.55° latitude (about 60 km at mid-latitudes), 85 atmospheric levels, and an upper boundary at 85 km near the mesopause. The ocean resolution is 0.25° with 75 quasi-horizontal levels. DePreSys3 uses a data assimilation scheme that nudges towards observed analyses in the atmosphere, ocean and sea ice. The ocean is nudged to monthly mean fields of 3-D temperature and salinity analyses, made from a global covariance ocean analysis<sup>56</sup>, using a 10-day relaxation timescale. Sea-ice concentration is nudged to monthly mean fields from the HadISST dataset<sup>57</sup>, using a 24 h relaxation timescale. The atmosphere is nudged to 6 h fields of ERA-interim<sup>58</sup> temperatures and winds with a 6-h relaxation timescale, from 2020 onwards we use ERA5 data adjusted to the ERA-Interim climatology. A 40 member ensemble is created by using different seeds to a stochastic physics scheme, as in GloSea5<sup>56</sup>.

We also briefly analyse the MPVI-SNAO relationship in the NCAR-SMYLE prediction system<sup>29</sup>, as this also has a long hindcast period (1979–2019) with 1st May start dates and a 20 member ensemble size. The system is based on the CESM2 climate model<sup>59</sup>.

To quantify SNAO skill in current operational seasonal prediction systems we use the same eight systems (UKMO, MF, CMCC, ECMWF, DWD, NCEP, ECCO, JMA) as used in ref. <sup>60</sup>. (to which we refer the reader for full details of the systems used) where hindcast data was downloaded from the Copernicus climate data store (<https://cds.climate.copernicus.eu/#!/home>) and from the IRI database (<https://iri.columbia.edu/our-expertise/climate/forecasts/seasonal-climate-forecasts/>) in August 2021. In total, 202 ensemble members were available for 1st May start date over the 1993–2016 hindcast period.

**Perturbation experiments.** To better isolate the role of the May stratosphere in driving SNAO variability we perform a simple perturbation experiment. We use the 2017 hindcast year as the basis as it has both a neutral MPVI and a neutral SNAO. We then perform two sets of three experiments, the first set switching the original 2017 1st May initial atmosphere initial conditions<sup>61</sup> for those in years that develop the strongest positive MPVI anomalies (1981, 2013, 2021), and the second set switching for those years that develop strongest negative MPVI anomalies (1997, 2011, 2019). The ocean and sea-ice initial conditions in all experiments remain unchanged from the 2017 original. All six experiments are run with 40 ensemble members from 1st May for four months. We, therefore, have 120 members in each of the positive and negative MPVI groups and the mean difference (positive minus negative MPVI) is calculated and tested for significance at the 90% confidence level using a one-sided Student's t-test.

**Late winter SSW years.** We follow previous studies<sup>47</sup> and define an SSW event based on ERA5 daily zonal mean zonal winds at

10 hPa and 60°N, over the years 1979–2022, based on the following criteria:

- (1) SSW identified as the first day on which the daily zonal mean zonal wind at 10 hPa and 60°N becomes easterly (<0 m/s)
- (2) Once an SSW is identified, 20 consecutive days with westerly winds must elapse before another central SSW can be identified
- (3) Cases when the winds are easterly, and do not return to westerly for at least 10 consecutive days before April 30th are treated as final warmings and hence not counted as SSWs

We find the following 12 late winter SSWs occurring between 1st February and 15th March:

[1979, 1980, 1981, 1984, 1988, 1989, 1999, 2001, 2002, 2007, 2008, 2018].

The composite difference between the mean of these years and the mean of the other 32 years is shown in Fig. 5. Significant differences in the means are identified using a one-sided Student's *t* test.

### Data availability

ERA5 reanalysis data was downloaded from the European Centre for Medium-Range Weather Forecasts (ECMWF), Copernicus Climate Change Service (C3S) at Climate Data Store (CDS; <https://cds.climate.copernicus.eu/>). Data from operational seasonal prediction systems are also available to download from the Copernicus data portal (<https://climate.copernicus.eu/seasonal-forecasts>) and the IRI database (<https://iri.columbia.edu/our-expertise/climate/forecasts/seasonal-climate-forecasts/>). The Met Office HadUK-Grid observed temperature dataset is available online (<https://www.metoffice.gov.uk/research/climate/maps-and-data/data/haduk-grid/datasets>). The NCAR-SMYLE prediction system data is available to download online (<https://www.earthsystemgrid.org/dataset/ucar.cgd.cesm2.smyle.html>). Met Office DePreSys3 data used in this study are available online (<https://doi.org/10.5281/zenodo.8421840>).

### Code availability

The computer code used to produce the figures is available from the corresponding author upon request.

Received: 31 March 2023; Accepted: 19 October 2023;

Published online: 06 November 2023

### References

1. Christidis, N., Jones, G. & Stott, P. Dramatically increasing chance of extremely hot summers since the 2003 European heatwave. *Nat. Clim. Change* **5**, 46–50 (2015).
2. Wulff, C. O., Greatbatch, R. J., Domeisen, D. I. V., Gollan, G. & Hansen, F. Tropical forcing of the Summer East Atlantic pattern. *Geophys. Res. Lett.* **44**, 11,166–11,173 (2017).
3. O'Reilly, C. H., Woollings, T., Zanna, L. & Weisheimer, A. The impact of tropical precipitation on summertime euro-Atlantic circulation via a circumglobal wave train. *J. Clim.* **31**, 6481–6504 (2018).
4. Ossó, A., Sutton, R., Shaffrey, L. & Dong, B. Development, amplification, and decay of Atlantic/European summer weather patterns linked to spring north atlantic sea surface temperatures. *J. Clim.* **33**, 5939–5951 (2020).
5. Sutton, R. T. & Hodson, D. L. Atlantic Ocean forcing of North American and European summer climate. *Science* **309**, 115–118 (2005).
6. Dunstone, N. et al. Skilful seasonal predictions of summer European rainfall. *Geophys. Res. Lett.* **45**, 3246–3254 (2018).
7. Folland, C. K. et al. The Summer North Atlantic Oscillation: past, present, and future. *J. Clim.* **22**, 1082–1103 (2009).
8. Hurrell, J. W., Kusnir, Y., Ottersen, G. and Visbeck, M. An overview of the North Atlantic Oscillation. The North Atlantic Oscillation: Climatic Significance and Environmental Impact. Geophysical Monograph, 134, American Geophysical Union, 1–35.2003
9. Buwen Dong et al. *Environ. Res. Lett.* **8**, 034037 (2013).
10. Hollis, D., McCarthy, M., Kendon, M., Legg, T. & Simpson, I. HadUK-grid—a new UK dataset of gridded climate observations. *Geosci. Data J.* **6**, 151–159 (2019).
11. Chronis, T., Raitsos, D. E., Kassis, D. & Sarantopoulos, A. The Summer North Atlantic Oscillation Influence on the Eastern Mediterranean. *J. Clim.* **24**, 5584–5596 (2011).

12. Hardt, B., Rowe, H. D., Springer, G. S., Cheng, H. & Edwards, R. L. The seasonality of east central North American precipitation based on three coeval Holocene speleothems from southern West Virginia. *Earth Plan. Sci. Lett.* **295**, 342–348 (2010).
13. Linderholm, H. W. et al. Interannual teleconnections between the summer North Atlantic Oscillation and the East Asian summer monsoon. *J. Geophys. Res.* **116**, D13107 (2011).
14. Scaife, A. A. et al. Skillful long-range prediction of European and North American winters. *Geophys. Res. Lett.* **41**, 2514–2519 (2014).
15. Baker, L. H., Shaffrey, L. C., Sutton, R. T., Weisheimer, A. & Scaife, A. A. An intercomparison of skill and overconfidence/underconfidence of the wintertime North Atlantic Oscillation in multimodel seasonal forecasts. *Geophys. Res. Lett.* **45**, 7808–7817 (2018).
16. Athanasiadis, P. J. A multisystem view of wintertime NAO seasonal predictions. *J. Clim.* **30**, 1461–1475 (2017).
17. Dunstone, N. et al. Skillful predictions of the winter North Atlantic Oscillation one year ahead. *Nat. Geosci.* **9**, 809–814 (2016).
18. Smith, D. M. et al. North Atlantic climate is far more predictable than models imply. *Nature* **583**, 796–800 (2020).
19. Matthew, P. et al. *Environ. Res. Lett.* **17**, 104033 (2022).
20. Franzke, C. & Woollings, T. On the persistence and predictability properties of north Atlantic climate variability. *J. Clim.* **24**, 466–472 (2011).
21. Hall, R., Erdélyi, R., Hanna, E., Jones, J. M. & Scaife, A. A. Drivers of north Atlantic polar front jet stream variability. *Int. J. Climatol* **35**, 1697–1720 (2015).
22. Scaife, A. A. et al. Tropical rainfall, Rossby waves and regional winter climate predictions. *Q.J.R. Meteorol. Soc.* **143**, 1–11 (2017).
23. Ineson, S. & Scaife, A. The role of the stratosphere in the European climate response to El Niño. *Nat. Geosci.* **2**, 32–36 (2009).
24. Scaife, A. A. et al. Seasonal winter forecasts and the stratosphere. *Atmos. Sci. Lett.* **17**, 51–56 (2016).
25. Wang, L. & Ting, M. Stratosphere-troposphere coupling leading to extended seasonal predictability of summer North Atlantic Oscillation and boreal climate. *Geophys. Res. Lett.* **49**, e2021GL096362 (2022).
26. Hersbach, H. et al. The ERA5 global reanalysis. *Q. J. R. Meteorol. Soc.* **146**, 1999–2049 (2020).
27. Baldwin, M. P. & Dunkerton, T. J. Stratospheric harbingers of anomalous weather regimes. *Science* **294**, 581–584 (2001).
28. Kidston, J. et al. Stratospheric influence on tropospheric jet streams, storm tracks and surface weather. *Nat. Geosci.* **8**, 433–440 (2015).
29. Yeager, S. G. et al. The Seasonal-to-Multiyear Large Ensemble (SMYLE) prediction system using the Community Earth System Model version 2. *Geosci. Model Dev.* **15**, 6451–6493 (2022).
30. Charney, J. G. & Drazin, P. G. Propagation of planetary-scale disturbances from the lower into the upper atmosphere. *J. Geophys. Res.* **66**, 83–109 (1961).
31. Hardiman, S. C. et al. Improved predictability of the troposphere using stratospheric final warmings. *J. Geophys. Res.* **116**, D18113 (2011).
32. Byrne, N. J. & Shepherd, T. G. Seasonal persistence of circulation anomalies in the southern hemisphere stratosphere and its implications for the troposphere. *J. Clim.* **31**, 3467–3483 (2018).
33. Haynes, P. H., McIntyre, M. E., Shepherd, T. G., Marks, C. J. & Shine, K. P. On the “downward control” of extratropical diabatic circulations by eddy-induced mean zonal forces. *J. Atmos. Sci.* **48**, 651–678 (1991).
34. Hardiman, S. C. & Haynes, P. H. Dynamical sensitivity of the stratospheric circulation and downward influence of upper-level perturbations. *J. Geophys. Res.* **113**, D23103 (2008).
35. Song, Y. & Robinson, W. A. Dynamical mechanisms for stratospheric influences on the troposphere. *J. Atmos. Sci.* **61**, 1711–1725 (2004).
36. Wittman, M. A. H., Polvani, L. M., Scott, R. K. & Charlton, A. J. Stratospheric influence on baroclinic lifecycles and its connection to the Arctic oscillation. *Geophys. Res. Lett.* **31**, L16113 (2004).
37. Scaife, A. A. et al. Climate change projections and stratosphere–troposphere interaction. *Clim. Dyn.* **38**, 2089–2097 (2012).
38. Kushner, P. J. & Polvani, L. M. Stratosphere–troposphere coupling in a relatively simple AGCM: the role of eddies. *J. Clim.* **17**, 629–639 (2004).
39. Butler, A. H., Charlton-Perez, A., Domeisen, D. I. V., Simpson, I. R. & Sjöberg, J. Predictability of Northern Hemisphere final stratospheric warmings and their surface impacts. *Geophys. Res. Lett.* **46**, 10578–10588 (2019).
40. Hauchecorne, A. et al. Stratospheric Final Warmings fall into two categories with different evolution over the course of the year. *Commun. Earth Environ.* **3**, 4 (2022).
41. Eade, R. et al. Do seasonal-to-decadal climate predictions underestimate the predictability of the real world? *Geophys. Res. Lett.* **41**, 5620–5628 (2014).
42. Scaife, A. A. & Smith, D. A signal-to-noise paradox in climate science. *npj Clim. Atmos. Sci.* **1**, 28 (2018).
43. Scaife, A. A. et al. Does increased atmospheric resolution improve seasonal climate predictions? *Atmos. Sci. Lett.* **20**, e922 (2019).
44. Hardiman, S. C. et al. Missing eddy feedback may explain weak signal-to-noise ratios in climate predictions. *npj Clim. Atmos. Sci.* **5**, 57 (2022).
45. Strommen, K. Jet latitude regimes and the predictability of the North Atlantic Oscillation. *Q. J. R. Meteorol. Soc.* **146**, 2368–2391 (2020).
46. Charlton, A. J. & Polvani, L. A new look at stratospheric sudden warmings. Part I: climatology and modeling benchmarks. *J. Clim.* **20**, 449–469 (2007).
47. Butler, A. H. et al. Defining sudden stratospheric warmings. *Bull. Am. Meteorol. Soc.* **96**, 1913–1928 (2015).
48. Bloxam, K. & Huang, Y. Radiative relaxation time scales quantified from sudden stratospheric warmings. *J. Atmos. Sci.* **78**, 269–286 (2021).
49. Rao, J., Ren, R., Chen, H., Yu, Y. & Zhou, Y. The stratospheric sudden warming event in February 2018 and its prediction by a climate system model. *J. Geophys. Res. Atmos.* **123**, 13,332–13,345 (2018).
50. Drouard, M., Kornhuber, K. & Woollings, T. Disentangling dynamic contributions to summer 2018 anomalous weather over Europe. *Geophys. Res. Lett.* **46**, 12537–12546 (2019).
51. Dunstone, N. et al. Windows of opportunity for predicting seasonal climate extremes highlighted by the Pakistan floods of 2022. *Nat. Commun.* **14**, 6544 (2023).
52. Rao, J. et al. Impact of the initial stratospheric polar vortex state on East Asian spring rainfall prediction in seasonal forecast models. *Clim. Dyn.* **60**, 4111–4131 (2023).
53. Lockwood, J. F. et al. Seasonal prediction of UK mean and extreme winds. Quarterly Journal of the Royal Meteorological Society, 1–13. Available from: <https://doi.org/10.1002/qj.4568>.
54. Williams, K. et al. The Met Office Global Coupled model 2.0 (GC2) configuration. *Geosci. Model Dev.* **88**, 1509–1524 (2015).
55. MacLachlan, C. et al. Global Seasonal forecast system version 5 (GloSea5): a high-resolution seasonal forecast system. *Q. J. R. Meteorol. Soc.* **141**, 1072–1084 (2015).
56. Smith, D. M. & Murphy, J. M. An objective ocean temperature and salinity analysis using covariances from a global climate model. *J. Geophys. Res.* **112**, C02022 (2007).
57. Rayner, N. A. et al. Global analyses of sea surface temperature, sea ice, and night marine air temperature since the late nineteenth century. *J. Geophys. Res.* **108**, 4407 (2003).
58. Dee, D. P. et al. The ERA-Interim reanalysis: configuration and performance of the data assimilation system. *Q. J. R. Meteorol. Soc.* **137**, 553–507 (2011).
59. Danabasoglu, G., Deser, C., Rodgers, K., and Timmermann, A. the CESM2 large ensemble dataset, climate data gateway at NCAR [data set], <https://doi.org/10.26024/kgmp-c556>, (2022).
60. Thornton, H. E., Smith, D. M., Scaife, A. A. & Dunstone, N. J. Seasonal predictability of the East Atlantic Pattern in late autumn and early winter. *Geophys. Res. Lett.* **50**, e2022GL100712 (2023).
61. Stockdale, T. N., Molteni, F. & Ferranti, L. Atmospheric initial conditions and the predictability of the Arctic Oscillation. *Geophys. Res. Lett.* **42**, 1173–1179 (2015).
62. Kanamitsu, M. et al. NCEP-DOE AMIP-II reanalysis (R-2). *Bull. Am. Meteorol. Soc.* **83**, 1631–1643 (2002).

## Acknowledgements

This work was supported by the Met Office Hadley Centre Climate Programme funded by BEIS and Defra. It was also funded by the Met Office Climate Science for Service Partnership (CSSP) China project under the International Science Partnerships Fund (ISPF).

## Author contributions

N.D. led the analysis and wrote the first draft of the paper with support from D.S. S.H. assisted with the perturbation experiments and S.I. with analysis of observed stratospheric warming events. All co-authors (D.S., S.H., L.H., S.I., G.K., C.L., J.L., A.S., H.T., M.T. and L.W.) contributed to the editing and writing of the manuscript.

## Competing interests

The authors declare no competing interests.

## Additional information

**Supplementary information** The online version contains supplementary material available at <https://doi.org/10.1038/s43247-023-01063-2>.

**Correspondence** and requests for materials should be addressed to Nick Dunstone.

**Reprints and permission information** is available at <http://www.nature.com/reprints>

**Publisher's note** Springer Nature remains neutral with regard to jurisdictional claims in published maps and institutional affiliations.



**Open Access** This article is licensed under a Creative Commons Attribution 4.0 International License, which permits use, sharing, adaptation, distribution and reproduction in any medium or format, as long as you give appropriate credit to the original author(s) and the source, provide a link to the Creative Commons license, and indicate if changes were made. The images or other third party material in this article are included in the article's Creative Commons license, unless indicated otherwise in a credit line to the material. If material is not included in the article's Creative Commons license and your intended use is not permitted by statutory regulation or exceeds the permitted use, you will need to obtain permission directly from the copyright holder. To view a copy of this license, visit <http://creativecommons.org/licenses/by/4.0/>.

© Crown 2023